Chinese Chemical Letters 35 (2024) 108458

Contents lists available at ScienceDirect

Chinese Chemical Letters

journal homepage: www.elsevier.com/locate/cclet

# Organic interfacial engineering of gold nanowires for selective glycerol electrooxidation

Zhe Wang, Qingling Hong, Boqiang Miao, Tianjiao Wang, Yu Ding*, Pujun Jin, Pei Chen, Yu Chen*

*Key Laboratory of Macromolecular Science of Shaanxi Province, Key Laboratory of Applied Surface and Colloid Chemistry (Ministry of Education), Shaanxi Key Laboratory for Advanced Energy Devices, School of Materials Science and Engineering, Shaanxi Normal University, Xi'an 710062, China*

ARTICLE INFO

*Article history:*
Received 14 March 2023
Revised 14 April 2023
Accepted 14 April 2023
Available online 16 April 2023

*Keywords:*
Glycerol electrooxidation reaction
Organic interface engineering
Gold-based nanomaterials
Electrocatalysis
Selectivity

ABSTRACT

The selective electrochemical conversion of glycerol into value-added products is a green and sustainable strategy for the biomass utilization. In this work, Au nanowires (Au-NW) modified with polyethyleneimine (PEI) molecule (Au-NW@PEI) is obtained by an up-bottom post-modification approach. Physical characterization, molecular dynamics simulation and density functional theory demonstrate that the loose-packed PEI monolayer firmly and uniformly distribute on the Au-NW surface due to the strong Au-N interaction. Electrochemical experiments and product analysis display that PEI modification significantly enhance the electro-activity of Au-NW for the glycerol electro-oxidation reaction (GEOR) due to the electronic effect. Meanwhile, the steric hindrance and electrostatic effect of PEI layer make the optimizing adsorption of intermediates possible. Therefore, the selectivity of C3 product glyceric acid over Au-NW@PEI is increased by nearly 20%. The work thus indicates that the rational design of metal-organic interface can effectively elevate the electro-activity and selectivity of Au nanostructures, which may have wide application in biomass development.



Over recent decades, the world glycerol production has sharply increased due to the fast development of biodiesel industry, resulting in the pressing requirement for re-utilization of glycerol (*i.e.*, a valuable byproduct in biodiesel industry). Recently, many advanced works have demonstrated that glycerol electro-oxidation reaction (GEOR) is an important anodic reaction in electrochemical system, which has widely potential applications in direct glycerol fuel cells and the electro-synthesis of value-added chemicals [1–4]. Among these chemicals, glyceric acid is well known for its benefits in medicine and skincare treatment. Glyceric acid and its derivatives have great potential as reagents for a variety of biological activities, including acting as base materials for functional surfactants and monomers for oligoesters or polymers [5,6]. Generally, noble metals (such as Pt, Pd and Au) based nanomaterials are excellent electrocatalysts for the GEOR due to their high electro-activity and durability [7–11]. Among them, Au based nanomaterials are especially attractive due to the high earth reserve and excellent anti-poisoning ability for CO intermediate [12–14].

Traditionally, morphology and component regulation are two efficient approaches for the electro-activity enhancement of Au based nanomaterials [15–21]. For example, Prof. Xu and co-workers synthesized the ultrathin Au nanowires (Au-NW) with Au(111) facets by $\alpha$-naphthol reduction method, which revealed boosted electro-activity for the oxygen electroreduction reaction due to high surface area, particularly one-dimensional (1D) anisotropy, and plentiful structural defects [22]. Prof. Du and co-workers synthesized two-dimensionally triangular AuCu alloy nanoprisms by a chemical reduction method, which revealed 3.9-fold electro-activity enhancement for the GEOR because of the electronic and bifunctional effects between Au and Cu [23]. Recently, the organic interface engineering of noble metal nanomaterials (*i.e.*, noble metal nanomaterials are modified by organic molecules) has emerged as an efficient stagey for enhancing their electro-activity and selectivity because of the electron/charge transfer between metal atoms and organic molecules as well as the steric effect of organic molecules at metal surface [24–34]. For instance, Prof. Chen and co-workers prepared Ir nanoparticles functionalized with 4-ethylphenylacetylene by ligand exchange method, which effectively boosted electro-activity of Ir nanocrystals for the oxygen electroreduction reaction because that the conjugated metal-ligand interfacial bonding interactions are in favor of adjustment

* Corresponding authors.
*E-mail addresses:* dingyu2527@gmail.com (Y. Ding), ndchenyu@gmail.com (Y. Chen).

https://doi.org/10.1016/j.cclet.2023.108458
1001-8417/

the electron density of Ir atoms [24]. Prof. Duan and co-workers synthesized sodium dodecyl sulfonate modified nickel hydroxide ($Ni(OH)_2$), which was highly efficient for the oxidation of cyclohexanone to adipic acid due to the favorable cyclohexanone transfer [29]. Prof. Sun and co-workers synthesized hydrophobic octadecanethiol modified $Fe_3P$ nanoarrays, which was highly active for the electro-catalytic $N_2$-to-$NH_3$ conversion due to optimized electronic structure and the hydrophobic character of alkanethiol [32]. These advanced works have demonstrated that the rational component/interface design can be used to adjust the adsorption energy of the key intermediates, thereby optimize the selectivity and electro-activity of the electrocatalyst.

In this work, we successfully constructed an organic interface at Au-NW surface by functionalizing Au-NW with polyethyleneimine (PEI) molecule (Fig. S1 in Supporting information). Herein, the strong interaction between Au and $-NH_2$ groups resulted in the spontaneous adsorption of PEI at Au atoms, which was internal driving force for the organic interface engineering of Au-NW. By means of the steric hindrance effect of PEI layer and strong Au-N interaction, the constructed PEI functionalized Au-NW (Au-NW@PEI) revealed improved electro-activity and selectivity for the anodic GEOR in alkaline medium compared to Au-NW without PEI.

In the typical synthesis, the PEI functionalized Au-NW (Au-NW@PEI) was easily obtained by ultrasonically dispersing Au-NW into PEI aqueous solution for 2 min and stirring for 2 h at room temperature. Herein, Au-NW with 5.3 nm diameter was easily achieved using $\alpha$-naphthol reduction method within 10 min (Fig. S2a in Supporting information) [27,35]. The morphology of Au-NW@PEI was visualized by scanning electron microscopy (SEM) and transmission electron microscopy (TEM). SEM image reveals that Au-NW@PEI has three-dimensionally (3D) network morphology with cross-linked pore structures, which are in fact constructed by tangled nanowires (Fig. 1a). Such 3D architecture can accelerate the mass transportation and electron communication in the course of electrochemical reactions. TEM image reveals that mean diameter of Au-NW@PEI is *ca.* 5.3 nm (Fig. 1b), which is identical with that of Au-NW without PEI (Fig. S2a). X-ray diffraction (XRD) pattern of Au-NW@PEI only reveals the diffraction peaks of Au crystal (Fig. 1c), which is exactly the same as Au-NW without PEI (Fig. S2b in Supporting information). Energy-dispersive X-ray spectroscopy (EDX) of Au-NW@PEI shows the obvious N elemental signal (Fig. 1d), suggesting the binding of PEI on the Au-NW surface due to the strong Au−N interaction. The density functional theory (DFT) calculation was carried out for the Au(111)-PEI system. The adsorption energy of a trimer of PEI on Au(111) is −1.4 eV, confirming the strong bond strength between PEI and Au.

X-ray photoelectron spectroscopy (XPS) measurement shows the strong N 1s signal, also suggesting the adsorption of PEI on

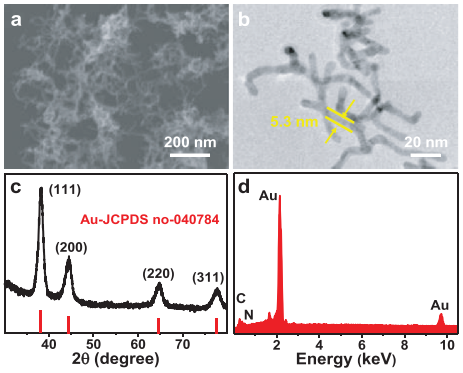


**Fig. 1.** (a) SEM, (b) TEM, (c) XRD and (d) EDX characterization of Au-NW@PEI.

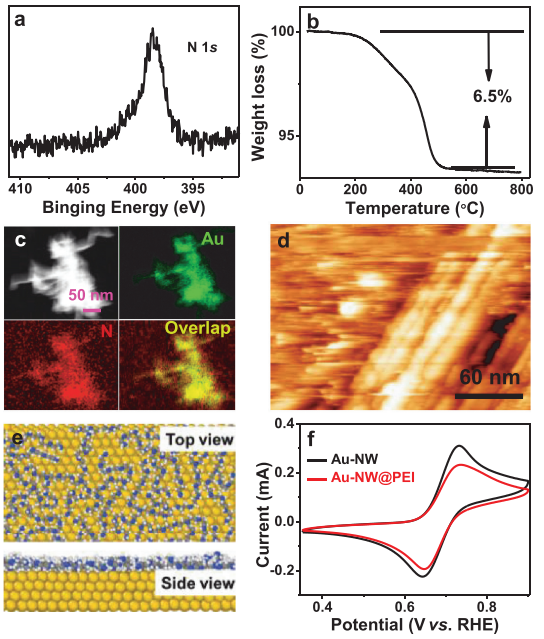


**Fig. 2.** (a) N 1s XPS spectrum, (b) TGA curve, (c) EDX mapping, (d) STM image of Au-NW@PEI. (e) Top view (above) and side view (below) of configurations of PEI on Au(111) surface. Herein, PEI molecule and Au(111) surface are displayed in ball and stick style. N, C, H and Au atoms are denoted by blue, gray, white, and yellow, respectively. (f) CV curves of Au-NW and Au-NW@PEI modified glassy carbon electrode in 10 mmol/L hydroquinone + 0.1 mol/L $HClO_4$ electrolyte.

Au-NW surface (Fig. 2a). Thermal gravimetric analyzer (TGA) curve of Au-NW@PEI reveals a weight loss of 6.5% because of the pyrolysis of PEI molecule at high temperature, suggesting the adsorption amount of PEI on Au surface is very small (Fig. 2b). The zeta potential measurement was performed to further confirm the adsorption of PEI on Au-NW surface. The zeta potential of Au-NW@PEI is +34.4 mV in 0.01 mol/L HCl solution. Such high zeta potential originates from the $-NH_3^+$ generation due to the protonation of $-NH_2$ at PEI in HCl solution. The existence of PEI endows Au-NW@PEI with well dispersion in an aqueous solution because of the strong electrostatic repulsion between positively charged Au-NW@PEI and hydrophilic of PEI molecules [36,37]. Indeed, Au-NW@PEI suspension can maintain stable within 10 days whereas Au-NW suspension only maintain stable for 10 min (Fig. S3 in Supporting information). EDX element mapping patterns reveal the uniform distribution of N and Au, suggesting the uniform distribution of PEI on Au-NW surface (Fig. 2c).

Scanning tunneling microscopy (STM) is a powerful technique for probing organic molecule on metal surface [38,39]. After the adsorption of PEI on the Au surface, large-scale synaptic structures are observed under ultrahigh vacuum conditions, displaying that PEI molecules can orderly self-assemble on the Au surface (Fig. 2d). STM measurement shows that the thickness of self-assembled PEI layer is about 0.97 nm (Fig. S4a in Supporting information). Considering that the vertical dimension of PEI molecule is about 0.7 nm (measured by PEI molecular model, Fig. S4b in Supporting information), the adsorption of PEI on the surface of Au may be monolayer and tiled distribution. The shaded areas in the middle of these PEI synapses layers are irregular channels, which confirms the loose distribution of PEI on the Au surface. Molecular dynamics (MD) simulations were performed to further investigate the adsorption of PEI molecules at Au surface. The top view image of optimized MD simulation displays that multiple branched PEI layer is at the loose lateral distribution, ascribing to the Au-N strong interaction. The side view image reveals the monolayer of the PEI, in agree-

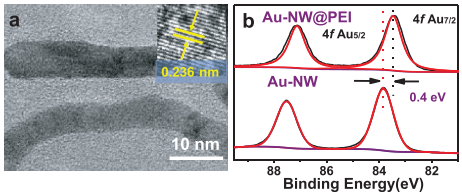


**Fig. 3.** (a) HRTEM image of Au-NW@PEI and (b) Au 4f XPS spectra of Au-NW@PEI and Au-NW.

ment with the STM result (Fig. 2e). As a result, a loose-packed PEI layer with abundant holes forms at the Au-NW surface, which allows the electrolyte and reactant access the uncovered Au atoms. Indeed, cyclic voltammetry (CV) measurements reveal that hydroquinone probe molecule can achieve the obvious electron communication at Au-NW@PEI electrode (Fig. 2f), confirming that the electrolyte and reactant can easily access Au-NW@PEI surface.

The fine structure of Au-NW@PEI was investigated by high resolution TEM (HRTEM) measurement. HRTEM image reveals the lattice spacing value (0.236 nm) of Au(111) facets (Fig. 3a), which is identical with Au-NW without PEI (Fig. S2c in Supporting information). The fact indicates the adsorption of PEI on Au-NW surface does not change the crystal structure of Au-NW. The electronic property of Au-NW@PEI was also explored by XPS. The doublet peaks of Au 4f XPS spectrum fitted to the metal Au species. Doublet peaks (83.8 and 87.5 eV) correspond to $4f_{7/2}$ and $4f_{5/2}$ peaks of metallic Au (Fig. 3b). The binding energy value ($4f_{7/2} = 83.4$ eV) of metallic Au on the Au-NW@PEI surface shifts negatively *ca.* 0.4 eV compared with that ($4f_{7/2} = 83.8$ eV) at Au-NW. The lone pair electrons of N atoms at $-NH_2$ groups can donate electrons to Au atoms, which is responsible for the negative shift of Au 4f binding energy [27,40].

Electrochemical properties of Au-NW and Au-NW@PEI were analyzed by CV in 0.1 mol/L $HClO_4$ electrolyte. In this work, all potentials were referenced to reversible hydrogen electrode (RHE). Both Au-NW and Au-NW@PEI show the obvious reduction peak of Au oxide at *ca.* 1.15 V (Fig. 4a). Generally, the electrochemical active area (ECSA) of Au nanomaterials can be measured by integral reduction peak area of Au oxides [41,42]. The ECSA of Au-NW and Au-NW@PEI are measured to be 38.6 and 31.8 $m^2/g$, respectively. After the PEI modification, Au-NW@PEI still has high ECSA, which confirms that the PEI layer does not completely cover Au-NW surface again.

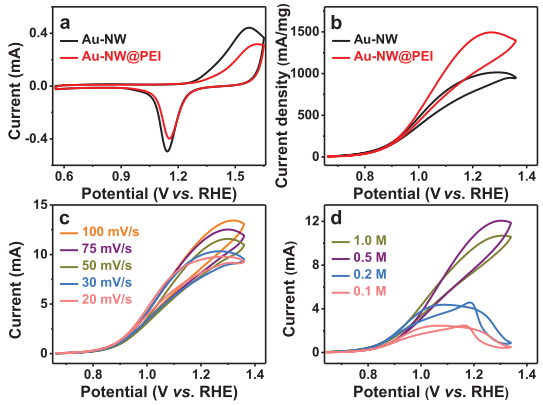


**Fig. 4.** (a) CV curves of Au-NW and Au-NW@PEI in 0.1 mol/L $HClO_4$ electrolyte at 50 mV/s. (b) Au mass normalized CV curves of Au-NW and Au-NW@PEI in 1 mol/L KOH + 0.5 mol/L glycerol solution at 50 mV/s. (c) Au-NW@PEI in 1 mol/L KOH + 0.5 mol/L glycerol electrolyte at different scan rates. (d) CV curves of Au-NW@PEI in 1 mol/L KOH electrolyte with different glycerol concentration at 50 mV/s.

The electro-catalytic activity of Au-NW and Au-NW@PEI for the GEOR were measured in the 1 mol/L KOH + 0.5 mol/L glycerol electrolyte (Fig. 4b). Both Au-NW and Au-NW@PEI show markable GEOR mass electro-activity. At the forward sweep direction, the onset potential and peak potential of GEOR locate at *ca.* 0.8 V and 1.3 V, respectively. At the reverse sweep direction, the reduction of the Au oxide allows the surface to reactivate for further oxidation of glycerol and reaction intermediates, resulting in the oxidation current at the reverse sweep direction [43]. Obviously, the forward GEOR peak current at Au-NW@PEI is much higher than that at Au-NW without PEI. Specifically, the GEOR peak current at Au-NW@PEI is 1496.7 mA/mg, which is 1.5 times of Au-NW (1016.5 mA/mg) at 1.27 V potential. Although the modification of PEI unavoidably decreases the electrochemical active area, the interaction between PEI and Au can regulate the electronic structure of Au active sites, which is more powerful on the GEOR activity.

To understand the high electro-activity of Au-NW@PEI, irregular Au nanoparticles (Au-NP) were prepared by potassium formate reduction method (Fig. S5 in Supporting information). ECSA and GEOR of Au-NP were also investigated by CV measurements (Fig. S6 in Supporting information). ECSA of Au-NP is only 9.7 $m^2/g$, which is 0.3 times than that of Au-NW. Obviously, the small diameter and 1D structure of Au-NW are responsible for its high ESCA value. Consequently, GEOR current (223.9 mA/mg) over Au-NP is much lower than that (1496.7 mA/mg) over Au-NW at 1.27 V, So the high electro-activity of Au-NW@PEI partly originates from the high area of Au-NW. The glycerol transmission performance over Au-NW@PEI was investigated by CV at different scan rates (Fig. 4c). The forward GEOR peak current increases with scanning rate. The linear relationship between the square root of the scan rate ($v^{1/2}$) and the forward GEOR peak current ($i_p$) reveals that GEOR at Au-NW@PEI is a diffusion-controlled process (Fig. S7 in Supporting information) [44]. Since the mass transfer process is important for the electrochemical process, the effect of reactant concentration on electro-activity was investigated by CV tests (Fig. 4d). CV curves display that Au-NW@PEI can achieve the highest GEOR peak current in 0.5 mol/L glycerol when the electrolyte concentration is fixed at 1 mol/L KOH. During the GEOR, the dissociative adsorption of glycerin on Au is the rate-determining step [45,46]. After increasing concentration, the mass transfer of glycerin is affected by the glycerol concentration, which leads to the shift of GEOR peak potential with glycerin concentration (Fig. S8 in Supporting information). After further increasing glycerol concentration, the GEOR current density decreases slightly, which can be ascribed to attenuation of ion transport properties due to increased viscosity of the electrolyte. Therefore, the 0.5 mol/L glycerol is an optimal concentration.

As a matter of fact, the ECSA normalized CV curves reflect the intrinsic electro-activity of the electrocatalyst. Obviously, the GEOR current density at Au-NW@PEI (4.7 mA/$cm^2$) is 1.8 times than Au-NW (2.6 mA/$cm^2$) at 1.27 V, indicating higher specific electroactivity (Fig. 5a). The results reveal that enhanced GEOR intrinsic

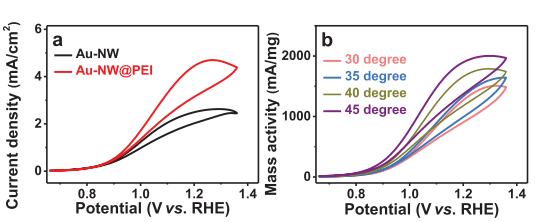


**Fig. 5.** (a) ECSA normalized CV curves of Au-NW and Au-NW@PEI in 1 mol/L KOH + 0.5 mol/L glycerol electrolyte at 50 mV/s. (b) Mass normalized CV curves of Au-NW@PEI in 1 mol/L KOH + 0.5 mol/L glycerol electrolyte at 50 mV/s at different temperatures.

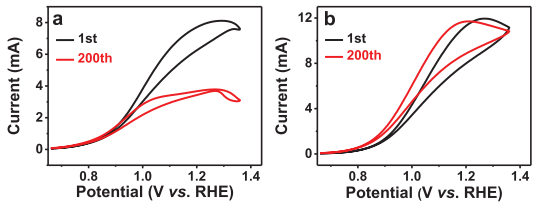


**Fig. 6.** The continuous CV curves of (a) Au-NW and (b) Au-NW@PEI in 1 mol/L KOH + 0.5 mol/L glycerol electrolyte at 50 mV/s.

electro-activity of Au-NW@PEI is highly relied on PEI modification. XPS results suggest that sufficient amount of PEI can serve as an electronic structure regulator (Fig. 3b), which is beneficial to regulate the electronic structure of Au active sites and optimize the adsorption energy of C3 intermediates [27,32]. Further CV tests at different temperatures are performed to investigate the GEOR electro-activity of Au-NW@PEI (Fig. 5b). Obviously, the GEOR current increase with reaction temperature. The apparent activation energy ($E_a$) is obtained from the linear regression of Arrhenius plot (Fig. S9 in Supporting information) [47,48]. $E_a$ of GEOR at Au-NW@PEI is 14.9 kJ/mol. Under the same experimental conditions, Ea of GEOR at Au-NW without PEI is measured to be 24.6 kJ/mol (Fig. S10 in Supporting information), much higher than Au-NW@PEI. The smaller $E_a$ means low energy barrier and advanced glycerol activation on Au-NW with the aid of PEI. For the GEOR, the dehydrogenation of glycerol is a rate-determining step, which can be effectively optimized by regulating the electronic structure [48,49]. So far, all electrochemical data has clearly revealed that PEI modification can improve the GEOR electro-activity of Au-NW due to the electronic effect.

The durability, an important parameter to estimate the feasibility of electrocatalysts, was evaluated by chronoamperometry measurements and continuous CV. We carried out the CV test (Fig. S11a in Supporting information) after chronoamperometric test (CA) at 1.15 V *vs.* RHE in 1 mol/L KOH solution (Fig. S11b in Supporting information). As observed, CV curve of Au-NW@PEI is almost unchanged after chronoamperometric test (red line), which proves the stability of Au-NW@PEI. In CV cycling durability test, the GEOR peak current at Au-NW decreases rapidly after 200 scanning cycles (Fig. 6a), which may cause by the strong adsorption of some intermediates [13]. In contrast, Au-NW@PEI is highly stable for the GEOR during continuous CV tests (Fig. 6b). Specifically, the mass electro-activity of Au-NW@PEI decay by 2.0% for GEOR after 200 cycles, which is much lower than that of Au-NW (53.1%). The chronoamperometry tests were also employed to identify the durability of Au-NW@PEI and Au-NW in terms of the decay rate and final mass current density after 5 h (Fig. S12 in Supporting information). At the initial stage, GEOR currents at Au-NW and Au-NW@PEI decay rapidly with an increase of time, which can be accounted for the rapid discharge behavior, the rapid depletion of $OH^-$ and strong adsorption of intermediates in the non-stirring condition [50,51]. Within the entire process, Au-NW@PEI shows much higher current density and slower downward trend than Au-NW without PEI for the GEOR. After 5 h CA test at 1.15 V, the GEOR at Au-NW@PEI reserves the 72.8% of initial current at the 100 s, much higher than that at Au-NW (45.1%), indicating improved durability of Au-NW@PEI.

All the durability tests have proven that Au-NW@PEI has excellent stability than Au-NW. According to GEOR mechanism, the strong adsorption carbon intermediates (C2* or C3*) are easily masked on the Au surface during the GEOR, resulting in poisoning of catalyst and current attenuation. The further structural analyses were conducted to explore the morphology stability of Au-NW@PEI after CA test. TEM characterization of Au-NW@PEI after CA test displays similar morphology and size to the previous one (Fig. S13a in Supporting information). TEM mapping images reveal that N element is still uniformly distributed on Au-NW surface (Fig. S13b in Supporting information), verifying the stability of PEI modification. As a result, the enhanced durability of Au-NW@PEI can be ascribed to the two aspects: (1) The change transferring between Au and $-NH_2$ on PEI optimizes the desorption behavior of intermediates on Au; (2) The stable three-dimensional network reduces the Ostwald ripening effect as well as the aggregation of Au-NW@PEI during the reaction.

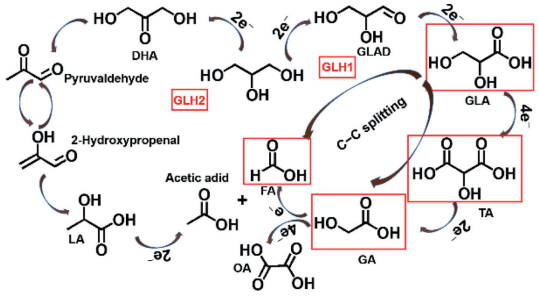


**Fig. 7.** The pathway of the GEOR.

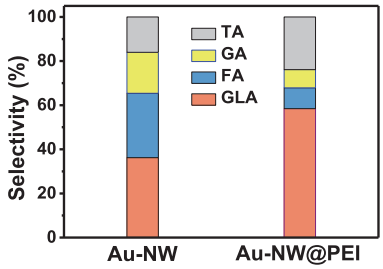


**Fig. 8.** The distribution of products of Au-NW@PEI and Au-NW after CA tests.

The carefully control of GEOR selectivity is challengeable due to the complex pathways (Fig. 7) [52]. Currently, two main mechanisms of the primary hydroxyl oxidation (GLH1) and secondary hydroxyl oxidation (GLH2) are propitious to GEOR. GLH1 process follows the path: first of all, glycerol must adsorb onto the electrocatalyst surface. Then, glycerol is oxidized the terminal carbon to obtain glyceraldehyde (GLAD). In a subsequent two-electron transfer, glyceraldehyde tends to be oxidized to glyceric acid (GLA) and tartronic acid (TA). After another C–C bond cleavage process, glycollic acid (GA), oxalate (OA), formate (FA), and carbonate form. GLH2 pathway endure the following process: after deprotonating two electrons, glycerol is initially oxidized to dihydroxy acetone (DHA). Then, undergo the base-catalyzed dehydration and tautomerization to form 2-hydroxypropenal, and then follow the Cannizzaro rearrangement to form lactate (LA). Herein, the selective oxidation of glycerol to more readily available C3 and C2 value-added products is highly desirable.

The selectivity of Au-NW@PEI and Au-NW for the GEOR were analyzed by high performance liquid chromatography (HPLC) method through the liquid products in the electrolyte after CA test. The product distributions over the Au-NW@PEI and Au-NW are shown in Fig. 8. The 4 compounds (TA, GA, FA and GLA) are detected, while OA is negligible. Therein, the yield rate of GLA obtained at 1.15 V in 2 h over Au-NW@PEI (192.0 μmol $h^{-1}$ $g^{-1}$) is higher than that of Au-NW (120.0 μmol $h^{-1}$ $g^{-1}$). The selectivity and yield rate of other products are shown in Table S1 (Supporting information). The experimental results indicate that Au-NW@PEI affords the higher selectivity for GLA (58.8%), which is approximately 1.6 times of Au-NW (36.2%). Based the pathway of GEOR, both Au-NW@PEI and Au-NW are more likely to follow the path

**Table 1**
The comparison of GEOR performance over Au-based catalysts.

| Catalyst | Selectivity | Potential (V *vs.* RHE) | Refs. |
|---|---|---|---|
| Au-NW@PEI | Glyceric acid (58.8%) | 1.15 | This work |
| Au/C | Glycolic acid (49.0%), glyceric acid (36.4%) | 1.31 | 2022 [53] |
| electrodeposited Au | Glycolic acid (51.9%), glyceric acid (38.5%) | 1.31 | 2022 [53] |
| Au films | Glycolic acid (41.2%) | 1.00 | 2021 [13] |
| $Ni_{0.9}Au_{0.1}$/C | Formate (100%) | 1.30 | 2020 [13] |
| Au@Ag nanoparticle | Glycolic acid (31.6%) | 1.10 | 2020 [54] |
| AgAu nanoparticles | Formate (66%), glycolate (32%) | 1.26 | 2020 [44] |
| Au nanoparticles | Dihydroxyacetone (26.83%), glyceraldehyde (14.01%) | 0.50 | 2019 [55] |
| AuAg nanoparticles | Formate (59.31%), glycolate (34.72%) | 1.13 | 2017 [56] |
| Au nanoparticles | Formate (40.96%), glycolate (21.33%) | 1.13 | 2017 [56] |

of GLH1. Meanwhile, the products were marked with a red box in Fig. 7. The Au-NW@PEI is prone to generate more GLA but less C2 products compared with the Au-NW, which means that Au-NW@PEI is more beneficial than Au-NW in promoting the C3 selectivity.

The high selectivity of GLA on Au-NW@PEI surface can be attributed to electronic structure regulation of PEI to Au surface, which can effectively regulate the adsorption energy of C3 products [13]. Meanwhile, PEI also acts as steric hindrance agent because of its special branching structure, which reduces the ability of glycerol at Au surface sites to form multi-bond intermediates, thus further improving the selectivity of C3 products [57]. As a result, the selectivity of C3 products (such as GLA) at Au-NW@PEI is much higher than that at Au-NW due to the existence of PEI, which restrains the generation of multiple-bonded intermediates by reducing the probability of finding neighboring Au sites [10,13]. In summary, the introduction of PEI influences the selectivity of C3 product over Au-NW by optimizing the active site microenvironment and restricting the C−C breakage of the glycerol relative to Au-NW, resulting in elevated production of C3 products at the applied potential. Based on pioneering literature for Au-based catalysts, Au-NW@PEI shows the high selectivity toward C3 products (Table 1). All the above results indicate that the organic engineering of Au-NW is beneficial to the electronic structure optimization of active sites and hence increase GEOR electro-activity and selectivity for C3 products.

In summary, polyethyleneimine functionalized Au nanowires (Au-NW@PEI) were successfully constructed by virtue of the strong interaction between $-NH_2$ groups and Au atoms. Such organic interface engineering endowed Au-NW with high GEOR electroactivity and 58.8% selectivity toward glyceric acid. PEI molecule optimized the adsorption of intermediates over Au-NW through electronic regulation. As a result, Au-NW@PEI obtained the significantly enhanced GEOR electro-activity compared to Au-NW. Considering the steric effect of PEI molecules on Au-NW surface could prevent multi-site adsorption, the C3 product glyceric acid selectivity of GEOR notably increased compared to Au-NW. This work revealed that organic engineering could effectively regulate electrocatalytic activity and selectivity through electronic effect and steric hindrance effect, which held promise for rational design of effective biomass catalyst system.

## Declaration of competing interest

The authors declare that they have no known competing financial interests or personal relationships that could have appeared to influence the work reported in this paper.

## Acknowledgments

This research was sponsored by National Natural Science Foundation of China (No. 22202130), China Postdoctoral Science Foundation (No. 2022M710088), Science and Technology Innovation Team of Shaanxi Province (Nos. 2023-CX-TD-27 and 2022TD-35), Fundamental Research Funds for the Central Universities (Nos. GK202202001 and GK202101005), Open Funds of the State Key Laboratory of Electroanalytical Chemistry (No. SKLEAC202207), and the 111 Project (No. B14041).

## Supplementary materials

Supplementary material associated with this article can be found, in the online version, at doi:10.1016/j.cclet.2023.108458.

## References

[1] L. Luo, W. Chen, S.M. Xu, et al., J. Am. Chem. Soc. 144 (2022) 7720–7730.
[2] H. Sheng, A.N. Janes, R.D. Ross, et al., Nat. Catal. 5 (2022) 716–725.
[3] S. Li, J. Lai, R. Luque, G. Xu, Energy Environ. Sci. 9 (2016) 3097–3102.
[4] J. Liang, Q. Liu, T. Li, et al., Green Chem. 23 (2021) 2834–2867.
[5] N. Kondamudi, M. Misra, S. Banerjee, et al., Appl. Catal. B: Environ. 126 (2012) 180–185.
[6] X. Zhou, H. Yan, X. Feng, et al., Green Chem. 23 (2021) 3664–3676.
[7] F. Yang, J. Ye, Q. Yuan, et al., Adv. Funct. Mater. 30 (2020) 1908235.
[8] A.M.S. Pembere, C. Cui, H. Wu, Z. Luo, Chin. Chem. Lett. 30 (2019) 1000–1004.
[9] Z. An, Z. Zhang, Z. Huang, et al., Nat. Commun. 13 (2022) 5467.
[10] S. Feng, J. Yi, H. Miura, et al., ACS Catal. 10 (2020) 6071–6083.
[11] M.S.E. Houache, K. Hughes, R. Safari, G.A. Botton, E.A. Baranova, ACS Appl. Mater. Interfaces 12 (2020) 15095–15107.
[12] F. Liao, X. Fan, H. Shi, et al., Chin. Chem. Lett. 33 (2022) 4380–4384.
[13] D. Kim, L.S. Oh, Y.C. Tan, et al., ACS Catal. 11 (2021) 14926–14931.
[14] M. Valter, E.C. dos Santos, L.G.M. Pettersson, A. Hellman, ACS Catal. 11 (2021) 3487–3497.
[15] X. Li, H. Zhao, J. Liang, et al., J. Mater. Chem. A 9 (2021) 6650–6670.
[16] Q. Shao, P. Wang, X. Huang, Adv. Funct. Mater. 29 (2019) 1806419.
[17] X. Yu, E.C. Dos Santos, J. White, et al., Small 17 (2021) e2104288.
[18] G. Zhang, Y. Wang, X. Wang, et al., Appl. Catal. B: Environ. 102 (2011) 614–619.
[19] T. Ahmad, S. Liu, M. Sajid, et al., Nano Res. Energy 1 (2022) e9120021.
[20] F.M. Souza, P. Bohnstedt, V.S. Pinheiro, et al., ChemElectroChem 6 (2019) 5396–5406.
[21] A.M. Verma, L. Laverdure, M.M. Melander, K. Honkala, ACS Catal. 12 (2022) 662–675.
[22] X. Jiang, X. Qiu, G. Fu, et al., J. Mater. Chem. A 6 (2018) 17682–17687.
[23] H. Xu, B. Yan, J. Wang, et al., J. Mater. Chem. A 5 (2017) 15932–15939.
[24] Y. Peng, Q. Liu, B. Lu, et al., ACS Catal. 3 (2021) 1179–1188.
[25] Y. Zhao, C. Wang, Y. Liu, D.R. MacFarlane, G.G. Wallace, Adv. Energy Mater. 8 (2018) 1801400.
[26] R. Li, J. Liang, T. Li, et al., Chem. Commun. 58 (2022) 2259–2278.
[27] Q. Xue, J. Bai, C. Han, et al., ACS Catal. 8 (2018) 11287–11295.
[28] Z. Zhong, L. Chen, L. Zhang, et al., Chin. Chem. Lett. 33 (2022) 3061–3064.
[29] Z. Li, X. Li, H. Zhou, et al., Nat. Commun. 13 (2022) 5009.
[30] J. Liang, Q. Liu, A.A. Alshehri, X. Sun, Nano Res. Energy 1 (2022) e9120010.
[31] T. Yang, J. Yang, X. Deng, et al., Angew. Chem. Int. Ed. 61 (2022) e202202957.
[32] T. Xu, J. Liang, Y. Wang, et al., Nano Res. 15 (2021) 1039–1046.
[33] Y. Zhang, D. Wang, S. Wang, Small 18 (2022) 2104339.
[34] S. Gong, F. Rao, W. Zhang, et al., Chin. Chem. Lett. 33 (2022) 4385–4388.
[35] Z.X. Ge, T.J. Wang, Y. Ding, et al., Adv. Energy Mater. 112 (2022) 2103916.
[36] Y. Ding, B.Q. Miao, Y.C. Jiang, et al., J. Mater. Chem. A 7 (2019) 13770–13776.
[37] S. Sun, B. Li, B. Fu, et al., Chin. Chem. Lett. 33 (2022) 5142–5146.
[38] Q. Li, J. Gao, Y. Li, et al., Nat. Commun. 9 (2018) 3113.
[39] G.R. Xu, C.C. Han, Y.Y. Zhu, et al., Adv. Mater. Interfaces 5 (2018) 1701322.
[40] S. Moniri, T. Van Cleve, S. Linic, J. Catal. 345 (2017) 1–10.
[41] E. Rouya, S. Cattarin, M.L. Reed, R.G. Kelly, G. Zangari, J. Electrochem. Soc. 159 (2012) K97–K102.
[42] A.T. Marshall, V. Golovko, D. Padayachee, Electrochim. Acta 153 (2015) 370–378.

[43] R. Boukil, N. Tuleushova, D. Cot, et al., J. Mater. Chem. A 8 (2020) 8848–8856.
[44] H. Yan, Q. Shen, Y. Sun, et al., ACS Catal. 11 (2021) 6371–6383.
[45] D. Xu, Y. Liu, S. Zhao, et al., Chem. Commun. 53 (2017) 1642–1645.
[46] B. Wang, L. Tao, Y. Cheng, et al., Catalysts 9 (2019) 387.
[47] M. Tao, N. Sun, Y. Li, S. Wang, X. Wang, Catal. Sci. Technol. 10 (2020) 207–214.
[48] M. Tinoco, S.F. Garcia, A. Villa, et al., Catal. Sci. Technol. 9 (2019) 2328–2334.
[49] K.M. Naik, K. Hashisake, T. Hamada, E. Higuchi, H. Inoue, J. Mater. Chem. A 10 (2022) 13987–13997.
[50] H. Pu, K. Dong, T. Zhang, et al., J. Mater. Chem. A 10 (2022) 10614–10624.
[51] D.M. Morales, D. Jambrec, M.A. Kazakova, et al., ACS Catal. 12 (2022) 982–992.
[52] H. Yan, S. Yao, J. Wang, et al., Appl. Catal. B: Environ. 284 (2021) 119803.
[53] L.S. Oh, M. Park, Y.S. Park, et al., Adv. Mater. (2022) 2203285.
[54] Y. Zhou, Y. Shen, J. Xi, Appl. Catal. B: Environ. 245 (2019) 604–612.
[55] Y. Zhou, Y. Shen, X. Luo, G. Liu, Y. Cao, Nanoscale Adv. 2 (2020) 3423–3430.
[56] L. Thia, M. Xie, D. Kim, X. Wang, Catal. Sci. Technol. 7 (2017) 874–881.